

UTDR Based Diagnosis for Membrane Filtration

J. Chen, *Member, IAENG* and Y.-C. Yang

Abstract—Current techniques available for the characterization of membrane are destructive, including scanning electron microscopy, mercury intrusion porosimetry and size exclusion of particles. An alternative technique based on ultrasonic frequency domain reflectometry (UTDR) that allows easy, non-invasive and real-time analysis of membrane morphology would be of significant value to the membrane industry. This study presents the technical detection results using UTDR, which is capable of diagnosing membrane fouling on various operation conditions. The detection technique is the combination of the wavelet transforms (WT) and the decision tree (DT). WT is used to represent all the possible types of transients in generated vibration signals. It is used for feature extraction and their relative effectiveness in feature extraction is compared. DT has been used for feature selection as well as for classification. Experimental results show that the algorithms are indeed efficient and effective.

Index Terms — Decision tree; Membrane fouling; Ultrafiltration; Wavelet analysis

I. INTRODUCTION

Membranes are used extensively for separation applications in industry. The energy efficient and modular nature of membranes has resulted in the replacement of several conventional separation processes in industry by more selective membrane. However, the most critical problem limiting further growth and wider applications of membrane-based liquid separations is fouling [1]. Fouling results from the deposition of retained particles, colloids, macromolecules, and/or salts on or in a membrane [2]. The increase in energy consumption and costs of membrane cleaning and replacement enlarge the adverse effects of fouling. Membrane fouling can occur on the membrane surfaces or within the pores of the membrane. The simplest approach for characterizing the membrane fouling is to measure clean water permeability's of the system before filtration, after filtration and after chemical cleaning. This can assess the resistance and reversibility of the fouling and the effectiveness of chemical cleaning. The method is simple but has the disadvantage of giving no information on fouling structure or morphology. Therefore, in order to gain a greater understanding of membrane fouling in terms of their structure, morphology and the sequential events of their

development, non-invasive techniques that enable the membrane fouling or the fouled membrane to be directly detected are strongly required.

In the past, optical methods have been applied to detection of structural heterogeneities of the deposit, but the lack of higher penetration depths and requirements of the specific system do potentially limit the application of optical techniques to membrane filtration [3]. Our previous work has shown that UTDR has the ability to provide rich information on membrane inside fouling structures as well as cake thickness [4]. While most attention has been given to improving ultrasound with integrated electronics for operators and engineers through the design of information signals [3], processing functionality is seldom considered in assessing the measured UTDR data and effectively identifying poor performance and faults. For example, Fig. 1 shows the ultrasonic echo of the filtered membrane for 5 typical operating conditions. The question is how to classify their operating conditions based on those ultrasonic signals only.

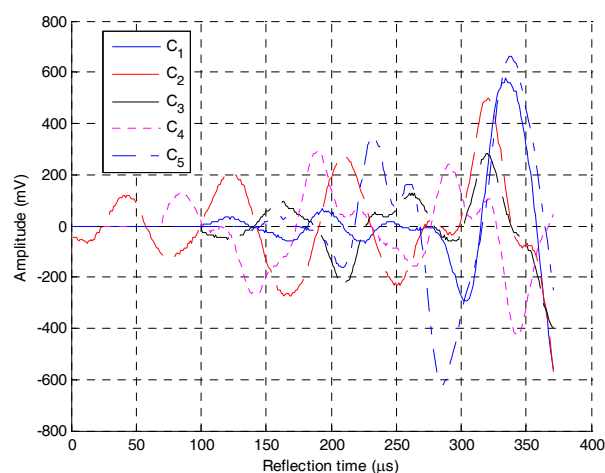


Fig. 1. The ultrasonic echoes of five different conditions in the filtered membrane

This paper addresses these issues using emerging data mining technology, including wavelet transforms (WT) and a decision tree (DT), to develop approaches to monitoring and diagnosis of the membrane filtration processes based on UTDR. WT is designed to address a particular frequency of interest. WT using differential signals has made it possible to observe the growth and change in density of the fouling layer [5,6]. The key idea is to apply DT induction algorithms to building the symbolic knowledge structure (IF-THEN rules) based on C4.5 [7] from WT data. This method summarizes UTDR data information into a compact form or a rule that

This work was sponsored in part by National Science Council, R.O.C.

J. Chen is with Department of Chemical Engineering, Chung-Yuan Christian University, Chung-Li, Taiwan 320, Republic of China (corresponding author to provide fax: 886-3-265-4199; e-mail: jason@wavenet.cycu.edu.tw).

Y.-C. Yang is with Department of Chemical Engineering, Chung-Yuan Christian University, Chung-Li, Taiwan 320, Republic of China.

helps us evaluate the fouling status of the current operation.

II. CHARACTERIZATION OF MEMBRANE MATERIALS USING UTDR

In all the experiments, 90mm diameter Millipore MF membranes with $0.05 \mu\text{m}$ VMWP are used. The filtration apparatus used for all the experiments is a 60.09cm^3 cell. The cell was operated in a dead-end mode forcing to separate phospholipids from the canola oil. The permeate flux was obtained by measuring the time to collect a certain weight of fluid using the A&D electric balance (Tokyo, Japan). The pressure of 3bar and the temperature of 30°C were kept constant in the normal operation during the experiment. The transmembrane pressure was monitored and adjusted by flow control valves and the downstream gas vacuum pump (Tokyo, Japan). As the module accommodates standard 76mm membrane discs, there is a possibility of investigating fouled membranes with a wide range of membranes. The membrane along with the filtration cake was removed from the module at the end-time points of filtration for the ultrasonic imaging. Then, a new membrane was used for each experiment.

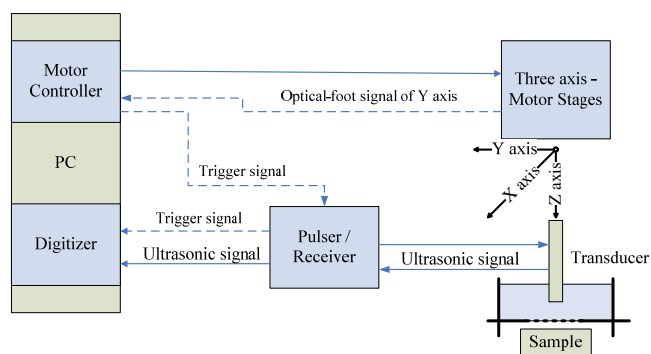


Fig. 2. Schematic representation of the ultrasonic measurement system

The ultrasonic measurement system shown in Fig. 2 consists of an ultrasonic transducer (NIH Ultrasonic Transducer Resource Center, USC), a high-voltage pulser/receiver (Model 5900PR, Panametrics, USA), a three dimensional motor stage, a motor controller (DMC-1842, Gaili motion control Inc, California, USA), and an analog-to-digital converter (PXI 5152, National Instruments, TX, USA). The three- dimensional motor stage comprises one piezo-ceramic motor (HR8, Nanomotion Ltd., Israel) and two servo motors (CM1-C-17L30A, Cool Muscle, Japan). The transducer is immersed in the commercial hydrogel directly casting on control or fouled membranes, and its relative distances, including length, width and depth to the membrane, can be precisely controlled by a motor. The pulser-receiver generates the required voltage signal that triggers the transducer to send an ultrasonic wave. The oscilloscope captures and displays the signal amplitude as a function of arrival time. Each set of ultrasonic signals generated consists of 800 data points. A computer (PC) is connected to the oscilloscope to store the data at the required intervals.

The ultrasonic pulse-echo method uses a short pulse of ultrasound generated by a transducer. The ultrasonic echoes

are reflected or scattered from various structures because of large interfaces between membrane and fouling or small inhomogeneities in the membrane/fouling objects. The pulse reflects from the opposite end and returns to generate a signal in the same transducer. Fig. 3 shows the ultrasonic echoes at a fixed position.

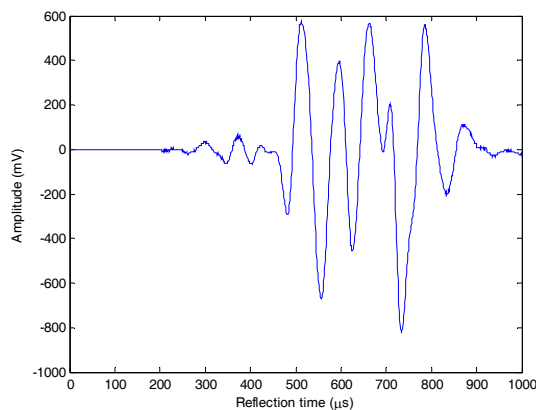


Fig. 3. An ultrasonic echo of the filtered membrane at a fixed position

When the transducer is fixed at a certain position, the echo signal set collected at the fixed point upon the observed zone can be expressed as

$$\mathbf{u} = [u^1 \ \dots \ u^z \ \dots \ u^Z]^T \quad (1)$$

where u^z refers to the amplitude of the ultrasonic signal at a reflection time of z . When the transducer moves zigzag as shown in Fig. 4, the echo signal set of the observed zone in the xy -plane can be expressed as

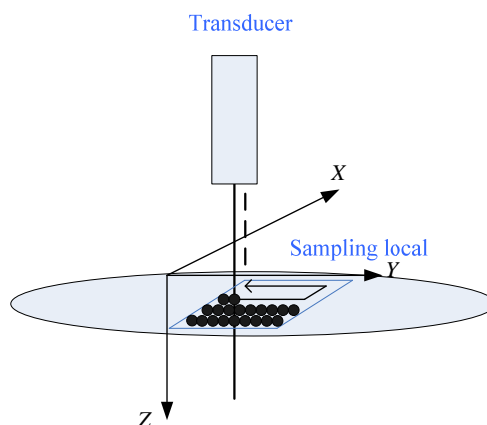


Fig. 4. The transducer moving zigzag over the whole plane

$$\mathbf{u}_{x,y} = [u_{x,y}^1 \ \dots \ u_{x,y}^z \ \dots \ u_{x,y}^Z]^T \quad (2)$$

$$x = 1, \dots, X, \ y = 1, \dots, Y$$

After the reflective signal upon a membrane is collected, the experimental data can be constructed in the form of the three-dimensional array. A three-dimensional array of data matrix \mathbf{U} with $X \times Y \times Z$ summarizes the whole testing

membrane structure. Therefore, at the fixed x , $Y \times Z$ with $y=1,2,\dots,Y$ measured along the y -axis direction at depth $z=1,2,\dots,Z$ intervals is the front view side shown in Fig. 5. Similar signals will be run at a number of intervals $x=1,2,\dots,X$ along the x -axis direction.

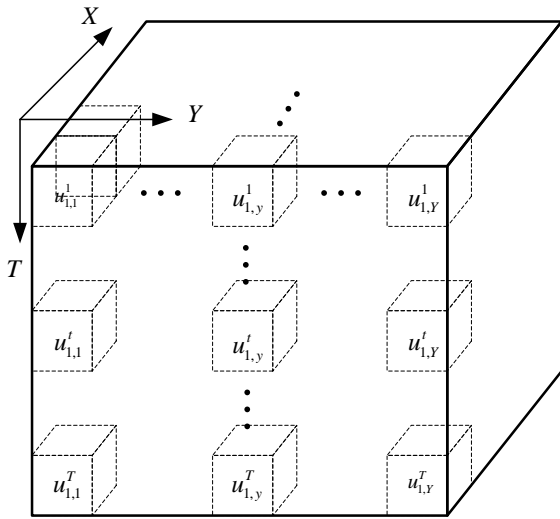


Fig. 5. three-dimensional array of data matrix summarizes the whole testing membrane structure.

III. FAULT DIAGNOSIS OF MEMBRANE FILTRATION USING UTDR

A. Wavelet Transform (WT) Analysis

To enrich the frequency resolution from ultrasonic transient signals, a discrete wavelet packet transform (DWPT) is applied here [8]. The basic idea of DWPT is to decompose a time series as a weighted sum of shifted and scaled versions of the wavelets that are suited for capturing the local behavior of non-stationary series, such as sharp changes with different characteristics of frequency at the same time intervals. To do this, the family of discrete wavelets with different scales and time parameters is given by $\psi_{m,n}(z) = a_0^{-m/2} \psi(a_0^{-m}t - nb_0)$, where m,n are integer. The wavelet coefficients are obtained by computing the correlation between the scaled and time shifted version of the wavelets and the analyzed part of the series from the ultrasonic signals. The coefficients in the linear combinations are computed by a factored or recursive algorithm. As a result, expansions in wavelet packet base have low computational complexity. The vector of coefficients at scale j is represented by

$$\begin{aligned} \mathbf{w}_{j,2n} &= \mathbf{H}_0 \mathbf{w}_{j-1,n} \\ \mathbf{w}_{j,2n+1} &= \mathbf{H}_1 \mathbf{w}_{j-1,n} \end{aligned} \quad (3)$$

where \mathbf{H}_0 and \mathbf{H}_1 are the orthonormal wavelet transform matrix for a low pass filter and a high pass filter respectively. They are gotten from a sequence of linear filtering operations. $\mathbf{w}_{0,0} = \mathbf{u}$. \mathbf{u} is the collections of the measured signals at equal space points. $\mathbf{w}_{j,2n}$ and $\mathbf{w}_{j,2n+1}$ are the projections on

the high-pass and the low-pass components respectively at scale j . For notational simplicity, we drop the index xy of the signal set ($\mathbf{u}_{x,y}$) here.

To reduce the dimensionality of the feature vectors and provide good class separation, the energies of the wavelet coefficients at scale J are used

$$s_n = \|\mathbf{w}_{J,n}\|, \quad n = 0, 1, \dots, 2^J - 1 \quad (4)$$

which is obtained by calculating the root mean square value of the wavelet coefficients [13].

Thus, each echo signal at the fixed location (x, y) consists of all the wavelet energy features at different frequencies,

$$\mathbf{s} = [s_0 \quad s_1 \quad \dots \quad s_{2^J-1}]^T \quad (5)$$

These energies are employed as elements of the feature vector. Eq.(5) is calculated only for the fixed location (x, y) in the xy -plane. For the whole plane, the average of $s_n(x, y)$ among all the locations is applied,

$$\bar{s}_n = \frac{1}{XY} \sum_{x=1}^X \sum_{y=1}^Y s_n(x, y) \quad (6)$$

where X and Y are the number of measured locations in the xy -plane. Thus, $\bar{\mathbf{s}} = [\bar{s}_0 \quad \bar{s}_1 \quad \dots \quad \bar{s}_{2^J-1}]^T$ can be regarded as a feature pattern that contains both spatial and frequency domain information. For notational simplicity, in the following discussion, the hat at the top of the notations $\bar{\mathbf{s}}$ and \bar{s} is neglected.

B. Classification of Operation States

The effectiveness and feasibility of the proposed auto-clustering method are presented with one frequency which contains all the experimental data in all the operation conditions. Fig. 6(a) shows the exact number of clusters is not clear in the original intensity energy histogram. Fig. 6(b) is the Gaussian smoothing result of Fig. 6(a) at initial $\sigma = 4.36$. In the figure, the circle points denote the center of each cluster. The spread parameters of smoothing are iteratively updated in Fig. 6(c), in which the input signal is smoothed at a larger spread parameter. Finally, all the operating conditions contain the divided eleven intervals. According to this auto-clustering algorithm, the cluster center $c_{n,c}$ can be computed. The collection of the energy data $s_{n,i}$, $n=1,2,\dots,2^J-1$, $i=1,2,\dots,I$ is partitioned into these clusters.

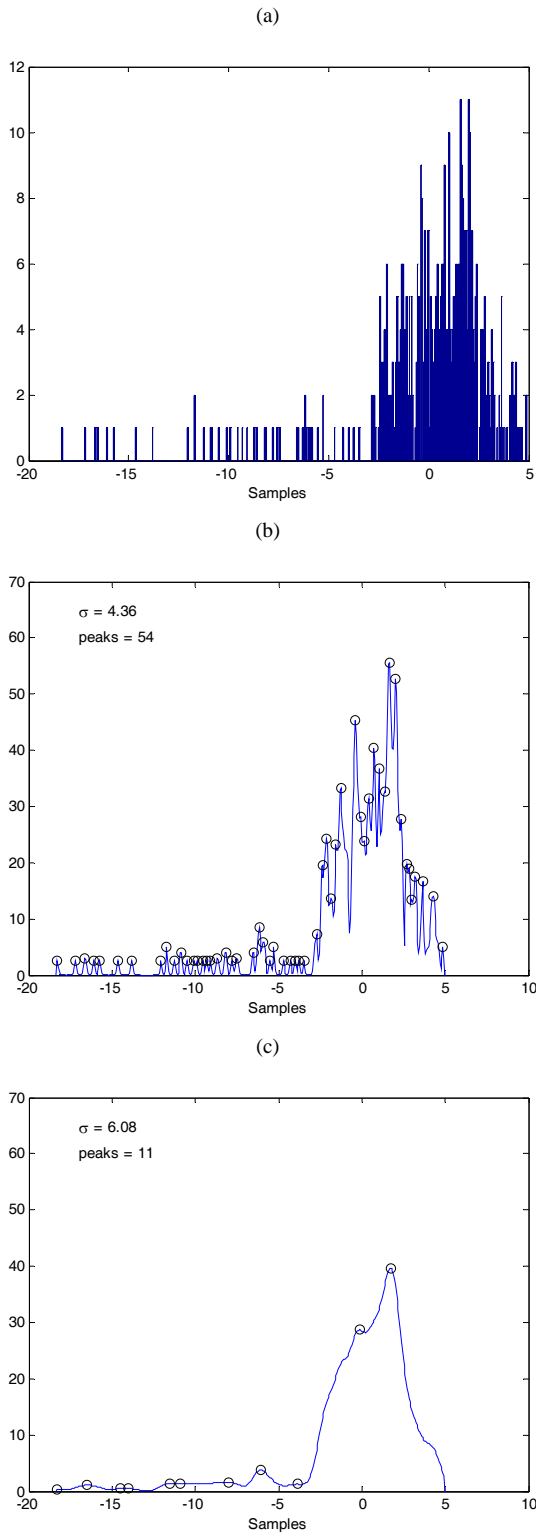


Fig. 6. Gaussian smoothing extracts the proper number of clusters: (a) histogram of original wavelet energy; smoothed signals from (b) to (c) at $\sigma = 4.36$ and 6.08 , respectively

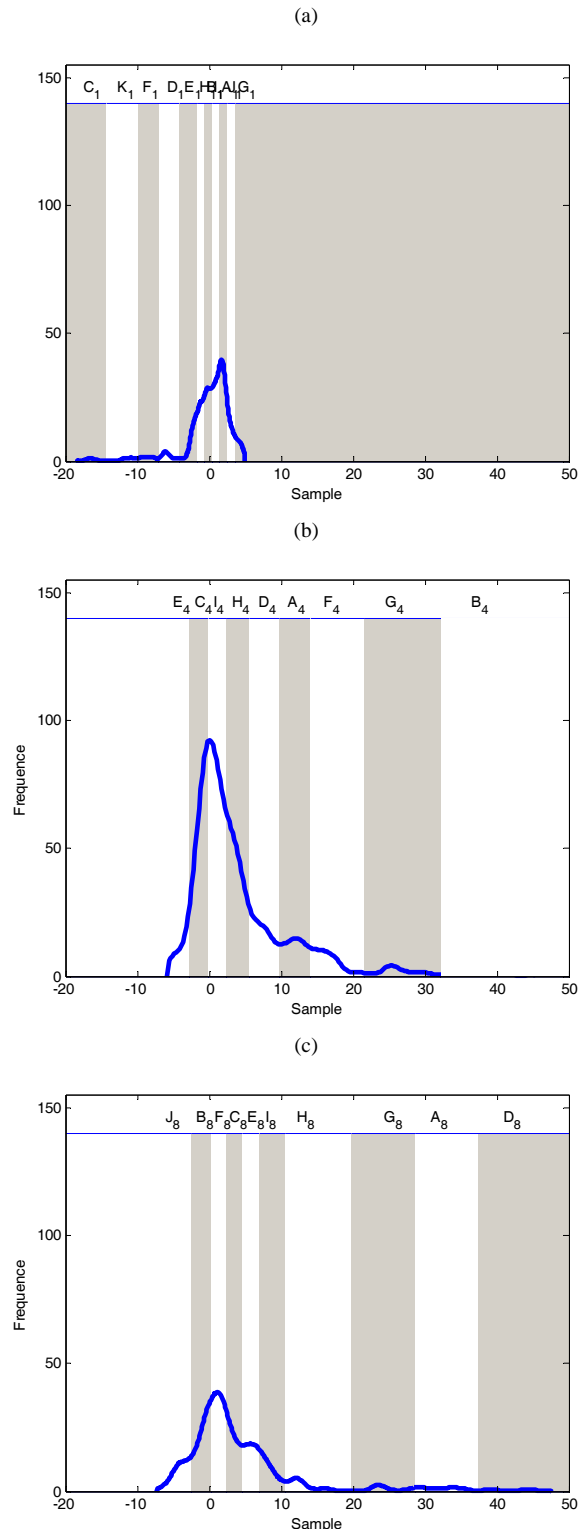


Fig. 7. Energy distributions at (a) the frequency scale $n = 1$, (b) the frequency scale $n = 4$, and (c) the frequency scale $n = 8$ in all the operating conditions. Each distribution is divided into several intervals with different shaded colors. Each interval is labeled by an attribute.

Because of the space limitation of the paper, Fig. 7 only shows the partition intervals of the energy distributions at frequency scale $n = 1$, $n = 4$ and $n = 8$ in the operating conditions from c_1 to c_5 .

C. Rule Extraction Using Decision Tree

After the frequency energies are characterized and the operation states are identified, it is necessary to find out how to generate knowledge which correlates the frequency energy scales with operational states. To do this, the data structure for the above clustering of all the study classes in Fig. 7 is shown in Table 1. In Table 1, given a number of samples, each row is described by a set of attributes

A classification scheme is designed for grouping the quantitative numbers (shown in Table 1(a)) into a number of classes (shown in Table 1(b)) so that instances within a class are similar in some respect, but they are distinct from other classes. The frequencies around the operation of a certain membrane filtration process may cover different frequency regions. DT can be built from given attribute sets. The tree can be converted into a set of IF-THEN rules. In contrast to the data-driven models (such as neural networks), one can understand the set of rules while numerical weights of neural networks cannot be easily deciphered.

Table 1. The data structure (a) with numerical values and (b) with the attributes of the membrane filtration for knowledge clustering. The rows represent observations from UTDR; the columns represent frequency scales.

(a)

Attribute Sample	1	2	8	Class ID
s_1	0.69	-0.38	1.48	1
s_2	-0.35	0.58	1.83	1
\vdots	\vdots	\vdots	\vdots	\vdots
s_{i-1}	0.75	-0.38	1.50	1
s_i	0.97	-1.46	39.58	2
s_{i+1}	1.43	-1.62	43.78	2
\vdots	\vdots	\vdots	\vdots	\vdots
s_{l-1}	2.10	-2.05	3.09	5
s_l	4.28	-4.06	0.77	5

(b)

Attribute Sample	1	2	8	Class ID
s_1	J_1	F_2	J_8	c_1
s_2	K_1	B_2	J_8	c_1
\vdots	\vdots	\vdots	\vdots	\vdots
s_{i-1}	J_1	F_2	J_8	c_1
s_i	J_1	C_2	F_8	c_2
s_{i+1}	A_1	C_2	F_8	c_2
\vdots	\vdots	\vdots	\vdots	\vdots
s_{l-1}	B_1	C_2	G_8	c_5
s_l	F_1	D_2	I_8	c_5

IV. EXAMPLES

In the present study, five different operating conditions shown in Table 2 was used, including 1 normal condition c_1

($30^\circ C$, $3bar$, $1g/100ml$), 5 abnormal conditions, namely high/low operating pressure (c_2 ($3.5 \sim 4bar$), c_3 ($2 \sim 2.7bar$)), high/low inlet concentration (c_4 ($1.3 \sim 1.5g/100ml$), c_5 ($0.5 \sim 0.7g/100ml$)), and the faults were created by changing the operating condition in order to keep the fault under control.

Table 2. Detail of the operation conditions under investigation

Class ID	Condition description
c_1	Normal operation
c_2	High operating pressure
c_3	Low operating pressure
c_4	High inlet concentration
c_5	Low inlet concentration

The diagnostic task of the membrane filtration is actually a problem of pattern classification and recognition. The crucial step of this problem is feature extraction. In this study, the ultrasonic signals in the space domain are transformed into the multi-scale data in the space-frequency domain using DWPT to enrich information. Each set of signals is divided into eight different frequency scales. The corresponding energy distributions at each frequency scale for all the operating conditions are computed. In fact, it is impossible to do the analysis as the volume of the above information is overwhelming. The proposed automatic classification is applied. Fig. 7 shows the energy signals at each frequency are grouped into several regions.

After the energy signals are characterized at each frequency and the operation condition is given, the next step is to find out the correlation between the frequency scales and the operation conditions. All the frequency scales of each data set in Fig. 7 constitute Table 1, in which each data set can be interpreted as an operation rule. DT developed for the case study is shown in Fig. 8 and it can be converted to production rules.

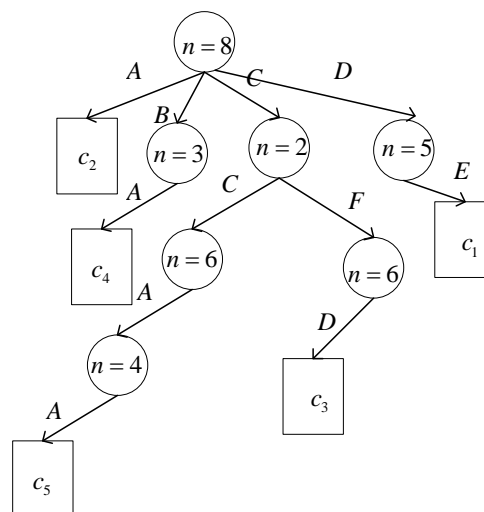


Fig. 8. DT is first constructed after the attribute variables of the frequency ($n = 8$) divided.

Due to the space limitation of the paper, only results of ten

samples for each condition are listed here. Case c_1 to c_5 for each filtration case in Table 3 represent the diagnosis outcome of ten samples. It is clear that classification accuracy of all the test samples is mostly correct.

Table 3. Results of the testing samples

Actual	Predicted					Overall detection rate
	c_1	c_2	c_3	c_4	c_5	
c_1	10	0	0	0	0	100%
c_2	0	9	0	0	0	90%
c_3	0	0	8	1	1	80%
c_4	1	0	0	9	0	90%
c_5	2	0	0	0	8	80%

V. CONCLUSION

UTDR technique is capable of membrane fouling noninvasively under realistic operating conditions. The ultrasonic technique can measure the changes on the membrane surface in a flat-sheet geometry. Although the transducers can be multiplexed and connected to a single remote digital oscilloscope-computer combination, a single transducer moves zigzag to collect all signals at any depth in the x-y-plane. The aforementioned ultrasonic system thereby enabling the reconstruction of the three dimensional data structure of the membrane is used to detect the structure of the membrane.

In this research the data mining technique which is the combination WT and DT from the UTDR signals of the fouling membranes is evaluated. It has been shown that the proposed method can effectively detect the fault types of the membrane fouling.

It is believed that the problem addressed here has not been fully studied before although it is important in membrane fouling diagnosis. A new practical method is provided to diagnose membrane fouling. The present research has clearly shown that the proposed method can be used effectively to diagnose membrane fouling from UTDR signals in the plate module; however, there are possibilities for implementation on other configurations, such as hollow fiber and spiral wound modules.

REFERENCES

- [1] G. Belfort, *Synthetic Membrane Processes*, G. Belfort (Ed.), Academic Press, Orlando, 1984.
- [2] M. Mulder, *Basic Principles of Membrane Technology*, Kluwer Academic Publishers, The Netherlands, 1991.
- [3] M. Legros, C. Meynier, R. Dufait, G. Ferin and F. Tranquart, Piezocomposite and CMUT arrays assessment through in vitro imaging performances, *Ultrason. Symp., 2008. IUS 2008. IEEE*, 2-5 pp.1142-1145, 2008.
- [4] L.-H. Cheng, Y.-C. Yang, J. Chen, Y.-H. Lin and S.-H. Wang, "A new view of membrane fouling with 3d ultrasonic imaging techniques: taking the canola oil with phospholipids for example," *J. Membr. Sci.* 372, pp. 134-144, 2011.

- [5] R.D. Sanderson, J. Li, D.K. Hallbauer and S.K. Sikder, "Fourier wavelets from ultrasonic spectra: a new approach for detecting the onset of fouling during microfiltration of paper mill effluent," *Environ. Sci. Technol.* 39, pp.7299-7305, 2005.
- [6] R. Sanderson, Jianxin Li, L. J. Koenb, L. Lorenzenb, "Ultrasonic time-domain reflectometry as a non-destructive instrumental visualization technique to monitor inorganic fouling and cleaning on reverse osmosis membranes," *J. Membr. Sci.* 207, pp.105-117, 2005.
- [7] J. R. Quinlan, *CA.5: Programs for Machine Learning*, Kaufmann, San Mateo, CA, 1993.
- [8] Z. Chen, Y. Shi, B. Jiao and H. Zhao, "Ultrasonic nondestructive evaluation of spot welds for zinc-coated high strength steel sheet based on wavelet packet analysis," *J. Mater. Process. Technol.* 209 pp.2329-2337, 2009.